Experimental investigation on underwater drag reduction using partial cavitation*

Bao Wang(王宝)[1], Jiadao Wang(汪家道)[1,†], Darong Chen(陈大融)[1], Na Sun(孙娜)[1,2], and Tao Wang(王涛)[1,3]

[1] *State Key Laboratory of Tribology, Tsinghua University, Beijing* 100084, *China*
[2] *School of Mechanical Engineering, Beijing Institute of Technology, Beijing* 100081, *China*
[3] *Science Technology on Vehicle Transmission Laboratory, China North Vehicle Research Institute, Beijing* 100161, *China*

(Received 11 December 2016; revised manuscript received 5 January 2017; published online 6 April 2017)

For underwater drag reduction, one promising idea is to form a continuous gas or discrete bubbly layer at the submerged surface. Owing to the lower viscosity of gas than of water, this could considerably reduce underwater drag by achieving slippage at the liquid–gas interface. This paper presents an experimental investigation on underwater drag reduction using partial cavitation. Dense hydrophobic micro-grooved structures sustain gas in the valleys, which can be considered as defects that weaken the strength of the water body. Therefore, partial cavities are easily formed at lower flow speeds, and the dense cavities connect to form a lubricating gas layer at the solid–liquid interface. The results indicate that the proposed method achieves drag reduction without any additional energy or gas-providing devices, which should stimulate the development of underwater vehicles.

Keywords: underwater drag reduction, hydrophobic, transverse microgrooved surface, partial cavitation

PACS: 47.85.lb, 47.55.Ca **DOI:** 10.1088/1674-1056/26/5/054701

1. Introduction

Drag reduction is significant in increasing the cruising speed and decreasing the energy consumption of partly or fully submerged vehicles. With the development of test and simulation techniques, several novel experimental and numerical approaches have boosted research in this field.[1–3] To pursue highly efficient underwater vehicles, several theoretical and experimental investigations have been carried out to investigate the structure of the boundary layer using methods such as a structured surface,[4–7] polymeric additives,[8–13] and traveling waves.[14] These methods of influencing the structure of the boundary layer can reduce the skin-friction drag of underwater vehicles.[15–18] However, a gas lubricating film or discrete bubbly layer at the solid–liquid interface can achieve much more effective drag reduction because of the much smaller viscosity of gas than of water. Superhydrophobic surfaces are a promising means of underwater drag reduction using gas because they can sustain air-pockets within surface structures while immersed in water.[19–23] The gas entrapped in gaps on the superhydrophobic surface enables the liquid–gas interface to replace the original solid–liquid interface, resulting in interfacial slippage that reduces the velocity gradient for underwater drag reduction.[24–26]

Although superhydrophobic surfaces are capable of sustaining air-pockets in their gaps and have demonstrated a noticeable slippage for underwater drag reduction, it is difficult to hold the gas stably, particularly when a liquid is flowing over the surface at high speed or liquid pressure.[27–31] This is because the gas initially on the surface is generally carried off by the flow or dissolved into the water.[27] No superhydrophobic surface has been shown to demonstrate its superhydrophobic properties underwater in realistic conditions.[32] Once the mechanical or thermodynamic equilibrium of the entrapped gas at the solid–liquid interface has been broken, the entrapped gas gradually disappears. Therefore, it is necessary to replenish the gas to ensure the continued presence of a lubricating gas film to achieve effective underwater drag reduction. Several active approaches attempt to replenish the gas removed from the surface. Gas injection is a simple and effective method of maintaining a lubricating gas film or bubbly layer at the solid–liquid interface[33,34] and the renewal of gas on a substrate can be achieved using an electric field or heating.[35–37] Although these approaches can achieve drag reduction using a gas layer, some gas-providing device or extra energy is required, which limits their practical applications.

One promising idea for underwater drag reduction by gas is supercavitation, which can create bubbles large enough to encompass the submerged object by cavitation effects, resulting in a lubricating gas layer around the underwater vehicle. Cavitation occurs when the local water pressure is less than the saturated vapour pressure[38,39] forming a cavity of vapour. To generate a cavity large enough to encompass a moving object for drag reduction, very high speeds (generally more than 100 m/s) are essential. In real applications, it is remarkably

*Project supported by the National Natural Science Foundation of China (Grant Nos. 51105223, 51075228, and 51605450) and the Tribology Science Fund of State Key Laboratory of Tribology of China (Grant No. SKLTKF15A02).

†Corresponding author. E-mail: jdwang@tsinghua.edu.cn

© 2017 Chinese Physical Society and IOP Publishing Ltd

difficult to achieve the high speeds needed to form a cavity covering an entire object, except for projectiles or very fast torpedoes.[40] However, the threshold of partial cavitation are not as strict as those of supercavitation, and are further weakened by defects in the water body. Hence, partial cavitation should be able to overcome the limitation of flow speed to enable real-world applications. Although partial cavitation has frequently been used for drag reduction by exposing part of the surface to gas,[40] further investigations on partial cavitation should be conducted to fully understand the mechanism for application.

In this study, the entrapped gas in a hydrophobic transverse microgrooved surface is used as the "defect" to reduce the breaking threshold to achieve partial cavitation at a lower flow velocity. Moreover, the dense distribution of the microgrooved structure is employed to connect the partial cavity, and direct observations are used to investigate the gas layer induced by the partial cavity. Finally, the drag reduction effect of this proposed method is verified in a water tunnel.

2. Materials and methods

2.1. Cavity formation

The formation of a cavity depends on a series of critical parameters, including the liquid velocity, pressure, and density. To model this, a non-dimensional parameter (cavitation number: σ_c) is often used to indicate the ease or complexity of cavity formation. This parameter can be described as

$$\sigma_c = \frac{p_\infty - p_c}{\frac{1}{2}\rho_l v_\infty^2}, \tag{1}$$

where p_∞ is the pressure at infinity, p_c is the cavity pressure, which generally refers to the saturated vapour pressure, ρ_l is the liquid density, and v_∞ is the main stream velocity in flowing water, which is the major influence on the cavitation number. From Eq. (1), as the flow velocity increases, the cavitation number decreases. Naturally, as shown in Fig. 1, with a relatively low flow velocity, no cavitation occurs and there is no cavity. When the flow speed reaches a critical value, the water body becomes broken, which can be considered as limited cavitation. At this point, the cavitation number reaches a critical value σ_{cr}. When $\sigma_{c=}\sigma_{cr}$, there are scattered bubbles on the surface; when $\sigma_c < \sigma_{cr}$, the cavitation phenomenon becomes aggravated and enters the developed cavitation status, whereby the moving object is partially located in the cavity. When the flow speed is sufficiently high, the cavity becomes large enough to fully encompass the moving object, and supercavitation is achieved.

According to Eq. (1), the higher flow speed is an essential for increasing cavity scale. Partial cavitation is the initial period of cavitation, so it is easily realized. Additionally, a previous investigation indicated that the bubble or impurity defects could weaken the threshold for cavitation.[38] However, it is difficult to achieve effective drag reduction with the scattered bubbles generated by partial cavitation, as shown in Fig. 2(a). To achieve underwater drag reduction by partial cavitation for general low-speed vehicles, dense defects are essential to connect the partial cavities, as shown in Fig. 2(b).

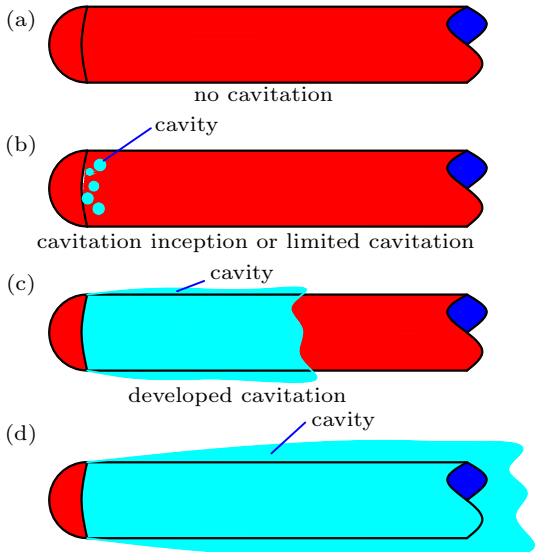


Fig. 1. (color online) Schematic diagram of cavitation, (a) no cavity, (b) limited cavitation, (c) developed cavitation, (d) supercavitation.

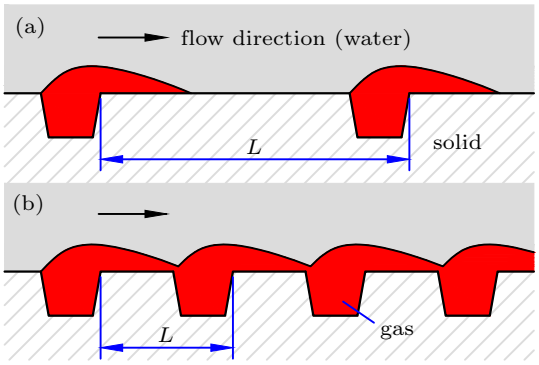


Fig. 2. (color online) Schematic diagram of the state at microgrooved structures. (a) The distance between two neighbouring grooves is large, so the bubbles are independent; (b) with dense microgrooved structures, the cavities can combine together.

2.2. Design and fabrication of surface structure

In previous investigations,[41,42] to sustain the gas at the surface as defect in the water body, a hydrophobic transverse microgrooved structure has been used to block the gas entrapped in the gaps. Additionally, regular dense valleys are designed to enhance the number of air-pockets. To sustain the gases stably in the grooves, the structure should be well designed to satisfy the mechanical equilibrium at the liquid–gas interface. The parameters of the designed structure are shown in Fig. 3.

In our experiments, the designed transverse microgrooves were fabricated on tubular samples with an outer diameter of 39 mm and length of 325 mm. The grooves were fabricated

by the turning method.[42] According to measurements of entrapped gas in a previous investigation, the geometry of the surface structures should be limited in certain conditions. The transverse microgrooved surfaces were constructed according to the parameters given in Table 1.

Additionally, the hydrophobicity of the surface is a key factor for sustaining gas in the gaps. To improve the water repellency of the original hydrophobic surface, a low-surface-energy material named fluoroalkylsilane (FAS-17) was applied to modify the grooved surface.[41–43]

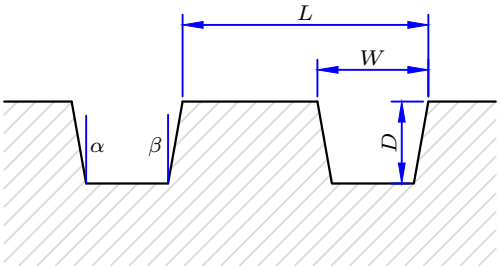


Fig. 3. (color online) Schematic diagram of surface topography. Profile of the microgroove has a cross-section with an isosceles trapezoidal shape of height (depth) D; front slope angle α, rear slope angle β; groove width W; and pitch L between two neighbouring grooves.

Table 1. Parameters of the microgrooved surface. S[a] denotes the sample number.

S[a]	Width/μm	Length/μm	Depth/μm	Front angle α/(°)	Back angle β/(°)
#1	12	30	13	4	4
#2	10	30	15	5	4
#3	10	30	5	4	6
#4	8	30	12	3	4
#5	7	30	15	4	7

2.3. Experimental equipment and measurement methods[41]

Optical observations and skin-friction drag tests were performed to evaluate the effectiveness of our approach. As shown in Fig. 4, water flowed perpendicularly over the hydrophobic transverse microgrooved surface in a water tunnel with a closed circulation system including a pump, anti-revolving section, honeycomb, and guide vanes.

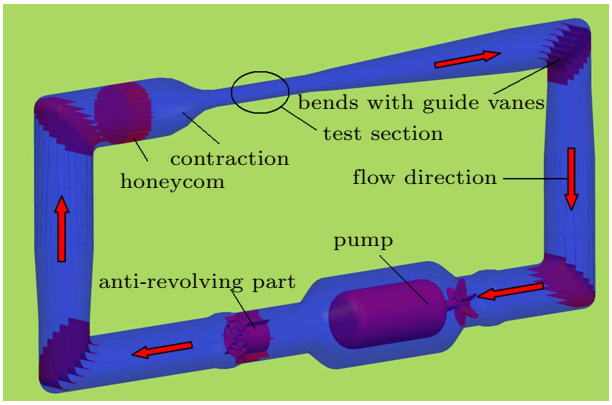


Fig. 4. (color online) Schematic diagram of the high-speed water tunnel.

The gas on the sample surfaces was visualized in a transparent (Plexiglass) test section of the water tunnel, as shown in Fig. 5. When the superhydrophobic surface is immersed in water, it becomes very bright,[44] as the reflectivity coefficient is greater for a gas–water interface than for the solid–water interface.

To confirm the drag reduction effect of this proposed method, we directly measured the skin-friction drag of tubular samples in this test section, as shown in Fig. 5. In the test section, the sliding parts, including the tubular sample and slip rings, were supported by the fixed components (a central axle, support frame, fairing, and tail). Because the total length of the sliding parts was designed to be less than the distance between the fairing and support frame, under the action of the flow, the sliding components could glide along the central axle, and displacement was transferred to the force sensor by the slip rings and pins. Finally, the force signal was acquired by a computer for data analysis. In this process, only the drag of the sliding parts can affect the recorded signal. Therefore, the friction of the surface being tested can be directly measured.[41]

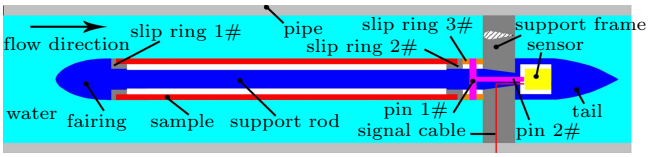


Fig. 5. (color online) Schematic diagram of test section in Fig. 4 for the skin friction drag test.

3. Results and discussion

3.1. Observation of entrapped gas

A series of optical observations were conducted to verify the effectiveness of the proposed method. The designed surfaces were modified with a simple coating of FAS-17. The surface water contact angle of the samples was only about 65°, which means that water could easily penetrate the grooves. In this case, when the samples were immersed in the water, the microgroove structures of the samples easily became wet, as shown in Fig. 6.

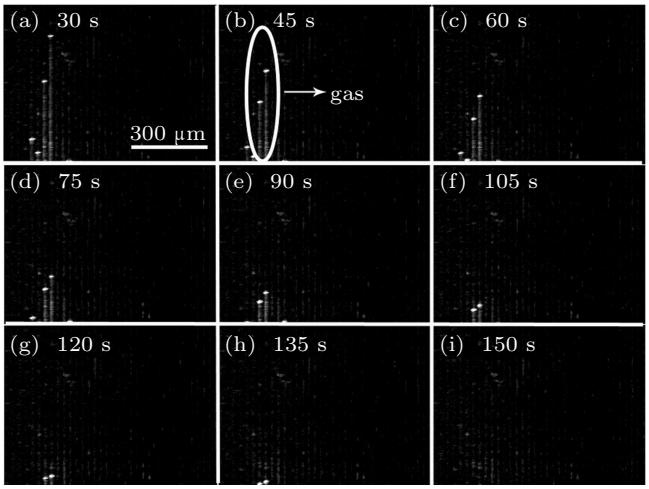


Fig. 6. Demonstration of wetting of microgrooves. (a) Samples have been immersed in water for 30 s, only 5% of the gas remains, with about 95% of the gas fraction in the microgrooves substituted for water; (b) after 45 s, 4% of the gas remains; (c) after 60 s, 3% of the gas remains; (d) after 75 s, 2.5% of the gas remains; (e) after 90 s, 1.5% of the gas remains; (f) after 105 s, 1% of the gas remains; (g) after 120 s, about 0.5% of the gas remains; (h) after 135 s, only a little fraction of the gas remains; (i) after 150 s, almost all of the gas in the microgroove structures has been substituted for water.

When the hydrophilic microgrooved surface was immersed in water, about 95% of the gas fraction in the microgrooved structures was substituted for water within 30 s, as shown in Fig. 6(a). After a short time, none of the gas remained because of the complete wetting of the surface by water, as shown in Fig. 6(i). When the grooved surfaces were modified with the low-surface-energy coating (FAS-17), they became hydrophobic. The contact-angle was tested to evaluate the hydrophobicity. Based on contact-angle measurements of the corresponding profile of water droplets (5 μL) on the smooth and microgrooved samples modified by this low-surface-energy material, we can ascertain that this modification achieves a contact angle of $115 \pm 2^\circ$ on the smooth surface and a contact angle of approximately 128° on the hydrophobic microgrooved surface, as shown in Fig. 7.[41]

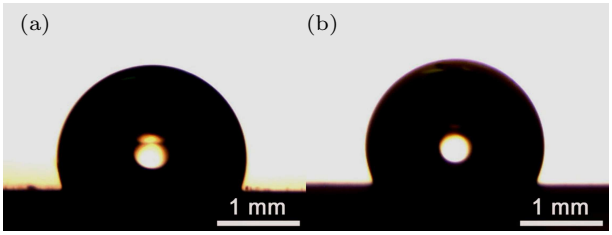


Fig. 7. (color online) Images of a water droplet (5 μL) on the different surfaces. (a) Smooth surface with FAS film, (b) microgrooved surface with FAS-17 film.

According to a previous investigation,[41] the intruding angle φ (the angle between the tangent of the three-phase junction and the horizontal line) was proposed as a critical parameter for the existence of entrapped gas underwater. To achieve Cassie's state, the intruding angle should be less than the maximum asperity slope angle. Based on the profile information of a water droplet on the surface shown in Fig. 7, the intruding angle for a droplet can be calculated as[41]

$$\varphi = \pi - \theta_0 + \arcsin\left\{\frac{f_{\mathrm{LG}}}{\lambda}\frac{1}{\sigma}\left[\frac{2\sigma}{R_{\mathrm{D}}} + \rho g R_{\mathrm{D}}(1-\cos\theta)\right]\right\}, \quad (2)$$

where θ_0 is the true contact angle (this can be considered as the contact angle on the original smooth surface coated with FAS-17, which is 115°); f_{LG} is the ratio of the projected area of the liquid–gas interface to the apparent contact area under the droplet; λ is the contact line density (the length of the contact line over the entrapped gas per unit apparent contact area); $2\sigma/R_{\mathrm{D}}$ is the pressure induced by the surface tension at the top of the droplet; R_{D} is the radius of the droplet; and θ is the apparent contact angle, 128°. Under the experimental conditions, $f_{\mathrm{LG}} = 33.3\%$; $\lambda = 6.67 \times 10^4$ m^{-1}; $\sigma = 0.0727$ N/m for a liquid density of 10^3 kg/m^3; and $R_{\mathrm{D}} = 1.2$ mm. Thus, the theoretical intruding angle of 65.5° given by Eq. (2) is less than the maximum asperity slope angle $(\pi\text{-}\alpha\text{-}\beta)/2$. Therefore, the initial gas can be entrapped in the proposed microgrooves of the designed surface, which was confirmed by the optical measurements shown in Fig. 8.[41,42]

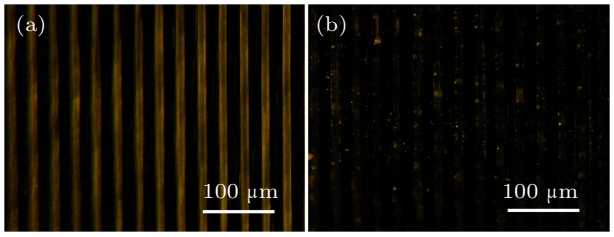


Fig. 8. (color online) Optical measurements of (a) the gas present in microgrooves modified with FAS-17 after immersion in water for 1 h and (b) the gas present in untreated hydrophilic microgrooves after immersion in water for 1 min.

3.2. Partial cavitation

In this experiment, when water flowed perpendicularly over the hydrophobic microgrooved surface at a low speed (down to 1 m/s), the results shown in Fig. 9 indicate that the gas-phase structure (corresponding to the bright area) continued to exist at the solid–liquid interface,[44] which confirms that hydrophobic grooves can hold gases in microstructures in flowing water. Furthermore, the gas on the hydrophobic transverse microgrooved surface was not static and instead fluctuated in the flowing water. In Fig. 9, shining sheets rather than scattered points indicates that a gas film can be achieved by this method. An alternating variation of bright (caused by gas) and dark lines can be observed, suggesting that cavitation occurs and the dense cavities connect to form a gas layer on the submerged surface because of the dense entrapped gas in the proposed structures. This gas layer almost covers the whole surface at low flow speeds (even at 1 m/s) without the need for any additional energy or gas-providing device. For the hydrophilic microgrooved surface (not modified by FAS-17), no

cavity was observed under the trial conditions. Without the entrapped gas, a much higher speed (far greater than that in our experiment) is needed to reduce the liquid pressure on the microstructured surface and break the water (cavitation). At a flow speed of 12 m/s in the water tunnel, which is less than the velocity required for cavitation, nothing was observed on the hydrophilic microgrooved surface in the test, which means that cavitation cannot occur at this flow speed.

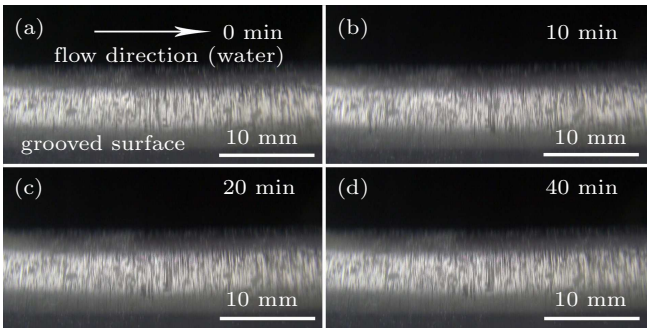


Fig. 9. Image of gas on the hydrophobic microgrooved surface in flowing water. (a) Initial time of measurement, 0 min, (b) 10 min, (c) 20 min, (d) 40 min.

As shown in Fig. 9, the fluctuating gas coverage on the hydrophobic transverse microgrooved surface remained fairly stable with immersion time in the flowing water. The fluctuation of the gas coverage with time shows that the gas continually disappears (corresponding to the areas changing from light to dark) and is replenished by the occurrence of cavitation (corresponding to the areas changing from dark to light) around the dense defects in flowing water. Therefore, this proposed method of dense partial cavitation can achieve a stable gas layer at the solid–liquid interface.

3.3. Drag reduction

The results in Fig. 8 indicate that the hydrophobic transverse microgrooved surface can hold gas in hydrophobic valleys in static water. When water flows perpendicularly over this surface, not only can the hydrophobic microstructures sustain entrapped gas, but cavities can also be generated without any additional energy or gas-providing devices due to partial cavitation. To evaluate the drag reduction effect of the gas film formed by partial cavitation, the underwater skin-friction drag of the prepared surface was tested in a miniature high-speed water tunnel. To evaluate the drag reduction performance, the relative drag reduction ratio is defined as

$$\lambda = \frac{F_s - F_c}{F_s} \times 100\%, \tag{3}$$

where F_s is the friction drag of a smooth surface and F_c is the friction drag of the sample (i.e., the friction of the transverse microgrooved surface). During this drag test, the state of the gas on the designed surface remained relatively stable because of the continuous generation and disappearance of the gas.

The experimental results in Fig. 10 show that the hydrophobic transverse microgrooved surface (#1) coated with low-surface-energy material achieves a steady drag reduction rate of about 13%, and that the drag reduction rate varies little with immersion time in the flowing water. This permanent drag reduction can be attributed to the relatively stable gas layer, because the gas continually generated by dense partial cavitation replaces the gas lost to the flowing water. However, the hydrophilic transverse microgrooved surface without FAS-17 coating failed to achieve underwater drag reduction, and even increases resistance. The increased drag compared with the hydrophobic transverse microgrooved surface can be attributed to the fact that cavitation cannot occur at this flow speed without entrapped gas acting as defects. Additionally, other surfaces with different geometric properties (sample #2–#5 in Table 1) were also measured, and achieved drag reduction rates of $10.10 \pm 0.18\%$, $14.02 \pm 0.15\%$, $8.40 \pm 0.25\%$, and $8.68 \pm 0.15\%$, respectively.

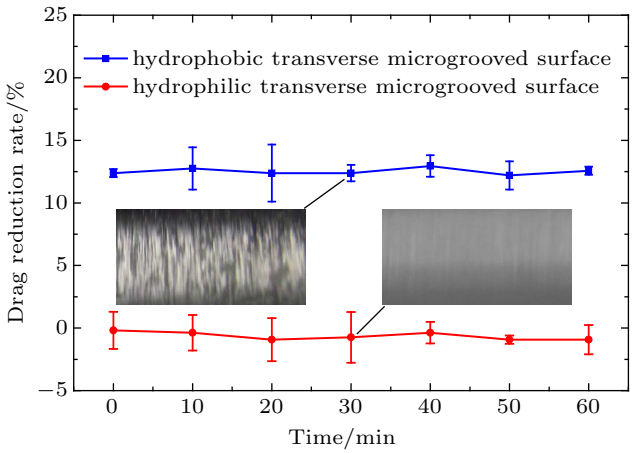


Fig. 10. (color online) Comparison of experimental drag reduction rate of transverse microgrooved surface with FAS-17 film and untreated grooved surface. A negative drag reduction rate indicates that the measured skin-friction drag is greater than that of the smooth surface.

4. Conclusions

Based on the design of "defects" on a surface, the threshold of cavitation was weakened, allowing the water body to be broken at lower flow speeds to form bubbles. A dense entrapped gas layer was achieved by a well-designed hydrophobic microgrooved surface. This dense entrapped gas allowed the scattered cavities to be connected to form a lubricating gas film on the designed surface. With sufficient gas at the solid–liquid interface, an effective reduction in drag was achieved by this optimized partial cavitation. Compared with active approaches for gas generation, the partial cavitation technique can form a stable gas film at the solid–liquid interface without any external energy supply or additional devices. The approach presented in this paper should open a new path toward achieving more effective underwater drag reduction using par-

tial cavitation and stimulate the development of related speed-enhancing and energy-saving technologies for underwater vehicles.

References

[1] Bechert D W, Bruse M, Hage W and Vander Hoeven J G T and Hoppe G 1997 *J. Fluid. Mech.* **338** 59
[2] Wang Y, Yu B, Cao Z Z, Zou W Z and Yu G J 2012 *Int. J. Heat Mass Tran.* **55** 4827
[3] Wang Y, Yu B and Sun S Y 2012 *Chem. Eng. Technol.* **35** 668
[4] Walsh M J 1983 *AIAA J.* **21** 485
[5] Rajabi H and Darvizeh A 2013 *Chin. Phys. B* **22** 088702
[6] García-Mayoral R and Jiménez J 2011 *Phil. Trans. R. Soc. A* **369** 1412
[7] Zhang D Y, Li Y Y, Han X, Li X A and Chen H W 2011 *Chin. Sci. Bull.* **56** 938
[8] Wang Y, Yu B, Wu X and Wang P 2012 *Int. J. Heat Mass Tran.* **55** 4849
[9] Wang Y, Shi H F, Fang B, Zakin J L and Yu B 2012 *Exp. Heat Transfer* **25** 139
[10] Li F C, Cai W H, Zhang H N and Wang Y 2012 *Chin. Phys. B* **21** 114701
[11] Mowla D and Naderi A 2006 *Chem. Eng. Sci.* **61** 1549
[12] Yang S Q and Dou G 2010 *J. Fluid Mech.* **642** 279
[13] Li F C, Wang L and Cai W H 2015 *Chin. Phys. B* **24** 074071
[14] Yao Y, Lu C and Si T 2011 *J. Hydrodynamic* **23** 65
[15] Gad-el-Hak M 1994 *AIAA J.* **32** 1753
[16] Wang Y, Yu B, Wu X, Wang P, Li F C and Kawaguchi Y 2014 *Adv. Mech. Eng.* **6** 574381
[17] Zheng X B, Jiang N and Zhang H 2016 *Chin. Phys. B* **25** 014703
[18] Choi J, Jeon W P and Choi H 2006 *Phys. Fluids* **18** 041702
[19] McHale G, Newton M I and Shirtcliffe N J 2010 *Soft Matter* **6** 714
[20] Zheng L J, Wu X D, Luo Z and Wu D 2004 *Chin. Sci. Bull.* **49** 1779
[21] Fang Y, Sun G, Wang T Q, Cong Q and Ren LQ 2007 *Chin. Sci. Bull.* **52** 711
[22] Bixler G D and Bhushan B 2012 *Soft Matter* **8** 11271
[23] Bhushan B 2012 *Langmuir* **28** 1698
[24] Gogte S, Vorobieff P, Truesdell R, Mammoli A, Van Swol F, Shah P and Brinker C J 2005 *Phys. Fluids* **17** 51701
[25] Tretheway D C and Meinhart C D 2002 *Phys. Fluids* **14** L9
[26] Crowdy D 2011 *Phys. Fluids* **23** 072001
[27] Sakai M, Nakajima A and Fujishima A 2010 *Chem. Lett.* **39** 482
[28] Poetes R, Holtzmann K, Franze K and Steiner U 2010 *Phys. Rev. Lett.* **105** 166104
[29] Aljallis E, Sarshar M A, Datla R, Sikka V, Jones A and Choi C H 2013 *Phys. Fluids* **25** 025103
[30] Govardhan R N, Srinivas G S, Asthana A and Bobji M S 2009 *Phys. Fluids* **21** 052001
[31] Forsberg P, Nikolajeff F and Karlsson M 2011 *Soft Matter* **7** 104
[32] Sun W Y and Kim C J 2013 *IEEE* 26*th International Conference on Micro Electro Mechanical Systems*, January 20, 2013, Taipei, Taiwan p. 397
[33] Karatay E, Haase A S, Visser C W, Sun C, Lohse D, Tsai P A and Lammertink R G H 2013 *P. Natl. Acad. Sci.* **110** 8422
[34] Sayyaadi H and Nematollahi M 2013 *Sci. Iran* **20** 535
[35] McCORMICK M E 1973 *Naval Eng. J.* **85** 11
[36] Lee C and Kim C J 2011 *Phys. Rev. Lett.* **106** 014502
[37] Vakarelski I U, Marston J O, Chan D Y C and Thoroddsen S T 2011 *Phys. Rev. Lett.* **106** 214501
[38] Joseph D D 1998 *J. Fluid Mech.* **366** 367
[39] Mohammadi A and Floryan J M 2013 *J. Fluid Mech.* **725** 23
[40] Xiang M, Cheung S C P, Tu J Y and Zhang W H 2011 *Ocean Eng.* **38** 2023
[41] Wang B, Wang J, Dou Z and Chen D 2014 *Ocean Eng.* **79** 58
[42] Wang B, Wang J D and Chen D R 2014 *Chem. Lett.* **43** 646
[43] Ding B, Ogawa T and Kim J 2008 *Thin Solid Films* **516** 2495
[44] Larmour I A, Bell S E J and Saunders G C 2007 *Angew. Chem.* **119** 1740